

Polycapillary based μ XRF station for 3D colour tomography

To cite this article: D. Hampai *et al* 2018 *JINST* **13** C04024

View the [article online](#) for updates and enhancements.

24TH INTERNATIONAL CONGRESS ON X-RAY OPTICS AND MICROANALYSIS
24–29 SEPTEMBER 2017
TRIESTE, ITALY

Polycapillary based μ XRF station for 3D colour tomography

D. Hampai,^{a,1} Yu.M. Cherepennikov,^{b,c} A. Liedl,^a G. Cappuccio,^a E. Capitolo,^a M. Iannarelli,^a C. Azzutti,^{a,d} Yu.P. Gladkikh,^e A. Marcelli^{a,f} and S.B. Dabagov^{a,g,h}

^aINFN - LNF, XLab Frascati, Via E. Fermi, 40, I-00044 Frascati (Rome), Italy

^bTomsk Polytechnic University, Lenin Avenue 30, Tomsk 634050, Russia

^cTomsk State University, Lenin Avenue 36, Tomsk 634050, Russia

^dUniv. Tor Vergata, Via Orazio Raimondo, 18, 00173 Roma

^eBelgorod State University, Belgorod, Russia

^fRICMASS, Rome International Center for Materials Science Superstripes,
Via dei Sabelli 119A, 00185, Roma, Italy

^gRAS P.N. Lebedev Physical Institute, Moscow, Russia

^hNational Research Nuclear University MEPhI, Moscow, Russia

E-mail: dariush.hampai@lnf.infn.it

ABSTRACT: The “Rainbow X-Ray” (RXR) experimental station at XLab Frascati of the Frascati’s National Laboratories (LNF) INFN is a dedicated station for X-ray fluorescence studies based on the use of polycapillary lenses in a confocal geometry. The flexible RXR layout allows investigating specimens of the dimensions ranging from several millimeters up to half meter and weighting up to several tens of kilograms. Compared to similar existing XRF stations, apart of the possibility for investigating large samples, the main advantage of this equipment is the detection system with two spectrometers optimized to work separately at high and at low X-ray energies. The confocal geometry combined with a 3-axes fine motion system makes possible 3D μ XRF elemental tomographic acquisitions (colour tomography). At present this station in operation at high XRF energies is used for cultural heritage and geological applications. We present and discuss here the analytical performances of this experimental station pointing out the advantages in different application areas.

KEYWORDS: Computerized Tomography (CT) and Computed Radiography (CR); X-ray fluorescence (XRF) systems

¹Corresponding author.

Contents

1	Introduction	1
2	RXR station: description and parameters	2
2.1	Confocal probe transverse cross-section	3
2.2	Z-axis confocal probe size	3
2.3	Detection limit	4
3	3D colour tomography	6
4	Conclusions	9

1 Introduction

X-ray fluorescence spectrometry (XRF) is a non-destructive technique providing both qualitative and quantitative information on solid samples [1]. Nowadays, it is one of the most common analytical tools for the elemental characterization of different samples at synchrotron radiation (SR) facilities. XRF methods aim in studying the elemental composition of a samples [2], as well as in collecting the images in a mapping mode to reconstruct spatial distribution of the detectable elements inside examined samples [3, 4]. Such techniques based on scanning procedures that translate either the source-detector system or the sample are flexible and offer different investigations opportunities.

At present, ultimate X-ray characterizations can be performed at SR facilities because they provide optimized radiation parameters for investigations (see, for instance, [5]). Namely, to perform advanced analysis it is necessary to deliver a high radiation flux to the sample with repeatable and controlled characteristics such as a spot size, beam profile, coherence, polarization, etc. However, the access to SR facilities is generally limited. Indeed, many dedicated experimental stations are overscribed. Moreover, considering conventional X-ray sources, the lack of optimized optics as well as hard X-ray detectors is the bottleneck for a wider use of the technique [6]. Nevertheless, the recent achievements in the design of X-ray optical devices make possible to obtain spatial resolution down to the micro-scale, even working with conventional X-ray tubes. Nowadays we can refer to technological advances associated to the availability of powerful compact X-ray sources and optics as well [7–15].

Among the most attractive and powerful X-ray optics well matching table-top X-ray sources, we can emphasize polycapillary optics, e.g., multi capillary-based lenses, semi-lenses, pillars, etc., the use of which has been continuously expanding since its invention [9, 16, 17]. These optics are characterized by strong focusing capability for X-ray beams with large divergences. Moreover, polycapillary optics can act as very efficient optical units both to collimate an X-ray beam and to transform a divergent X-ray beam into a quasi-parallel one [18, 19].

The XLab Frascati (XlabF) laboratory is the unique Italian laboratory dedicated to the design, manufacture and characterization of X-ray and neutron polycapillary optics [20, 21]. Additionally, since the beginning, this laboratory has been involved in the studies of customized source-optics-detector layouts for advanced X-ray spectroscopy devices [2, 21] and for microscopy applications based on polycapillary optics as well [22].

Recently, a new experimental layout, the “Rainbow X-Ray” (RXR) station, has been designed and has been commissioned at XlabF. In this work we present its characteristics together with the analysis of various samples.

2 RXR station: description and parameters

The RXR unit is a rather compact experimental apparatus dedicated to the research on 2D/3D X-ray micro-fluorescence (μ XRF) spectroscopy [23]. Its main parameters are characterized by a probe size ranging from 70 to 80 μm and by an excitation energy from 6 to 30 keV (the low energy can be optionally decreased to approximately 1 keV). This setup allows various experimental combinations; for instance, we can deal with the measurements for total reflection XRF analysis (TXRF) of a sample containing various elements at low concentrations ([21] and refs. therein). The RXR layout is based on a confocal geometry design [23] that allows the users to perform elemental depth profiling for different types of the samples. Moreover, the confocal approach simplifies the measurement procedure and allows discriminating depth-dependent signals from high to low Z elements. In addition, it avoids the negative superposition of images [24, 25].

The RXR setup is composed by two dedicated polycapillary optical elements (figure 1). A full-lens focuses the incident beam to the sample position, while the second one optimized for the energy range of 6–30 keV concentrates the fluorescent radiation onto the detector.

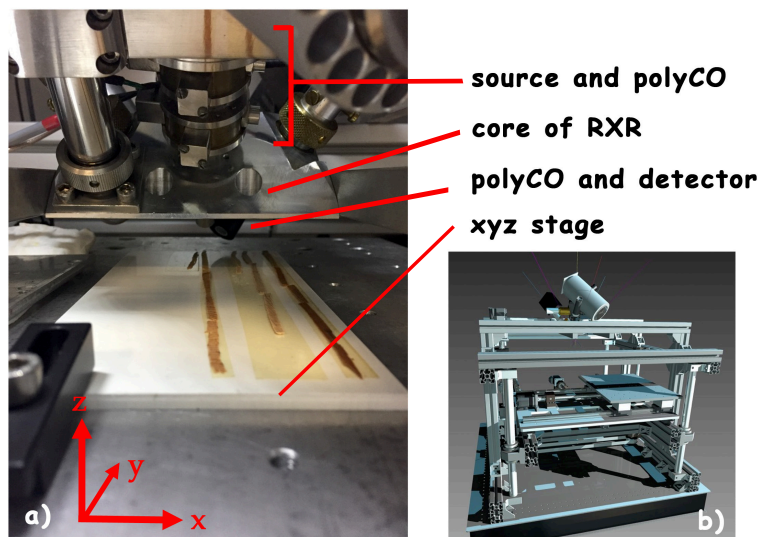


Figure 1. A photograph showing the interior of the RXR apparatus. The measurement head (at the top) and the sample holder stage (below) with wood samples under analysis can be clearly recognized.

The experimental layout of the station includes a focusing polycapillary lens with a $90\ \mu\text{m}$ FWHM spot size matching the Mo X-ray tube (Oxford Apogee 5000), a detector combined with a dedicated semi-lenses (from X-Channel Techn.), an alignment system and an optical microscope with a CCD camera (Basler acA750-30gc). To align the sample in the vertical plane and to scan the surface we use a laser profilometer with a spatial resolution of $10\ \mu\text{m}$ (Microspilon NCDT 1401 [26]). The software adopted for control instrumentation and data acquisition is based on LabVIEW [21, 23].

Since the polycapillary optics has optimal energy range, the actual detector is matched with a semi-lens in the energy range of 6–30 keV. This layout allows performing the fluorescence 2D/3D elemental mapping starting from the Fe element. The SDD detector has a working area of $25\ \text{mm}^2$ [27], and is equipped with a Be window optimized for high-energy radiation.

2.1 Confocal probe transverse cross-section

The RXR facility has been designed to be a really flexible instrument enabling the users to perform multiple measurements on different type of samples. Moreover, it provides a micro-fluorescence analysis with the possibility of both surface and volumetric mapping (3D mapping). To understand real capabilities of this instrument, below we describe its analytical and imaging tools.

Evaluation of the spatial resolution, along the three axes xyz , is directly correlated with the measurement of the confocal probe dimension [28, 29]. In order to obtain the confocal ellipsoidal dimensions, the measurements in the horizontal plane were performed with a $40\ \mu\text{m}$ Rh-Au wire, while in the perpendicular axis — of a $5\ \mu\text{m}$ Au sheet. The minimum concentration sensitivity was measured through a NIST standard as a function of fluorescence radiation energies. Finally, the complete analysis allows us getting a 3D tomography sample image characterized by morphological informations integrated by elemental composition details. In other words, we can use the RXR unit to get, so-called, “colour” tomography of our samples.

We collected a μXRF surface scan along the plane containing the wire (see figure 2) with the source operating conditions were fixed at 45 kV voltage and 0.95 mA current. A 1 mm linear scan was performed at $10\ \mu\text{m}$ step with an acquisition time of 60 s for each step. The Gaussian fit for the peak of the XRF curve in the xy plane (figure 2) returns a horizontal dimension of $77.4\ \mu\text{m}$.

Without errors and with a small step scan ($\ll 40\ \mu\text{m}$), the wire profile should have a squared shape $40\ \mu\text{m}$ wide. Since the step size is comparable ($10\ \mu\text{m}$) with the wire dimension, the experimental profile shows a smoothed square shape with a FWHM of about $60\ \mu\text{m}$ (accounting for the $40\ \mu\text{m}$ size of the wire and $20\ \mu\text{m}$ for both size). The difference Δ between the experimental value and the expected FWHM is $\sim 17.4\ \mu\text{m}$. This amount can be referred as the additional experimental contribution due to our confocal probe system.

2.2 Z-axis confocal probe size

To evaluate the probe dimension along the z -axis we carried out a similar scan in the vertical direction by using a gold sheet of $5\ \mu\text{m}$ thickness. The X-ray source parameters were the same of the previous test and the measurements were performed at 60 s acquisition time per point. The scan range of 2 mm with a step of $10\ \mu\text{m}$ was applied. In figure 3 the counts profile in the region of interest (ROI) for the iron peak is shown. The beam in the confocal spot forms an ellipsoidal focus. Its distribution

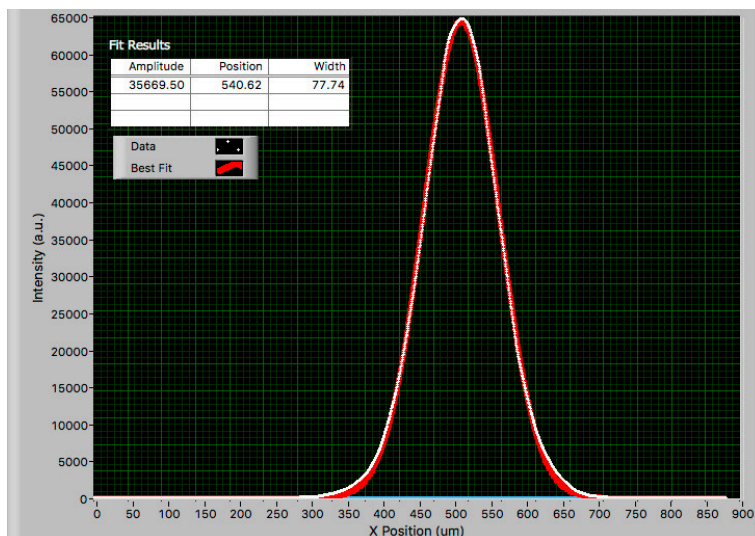


Figure 2. μ XRF results from a wire of Rh-Au of 40 μm measured along 1 mm with a step of 10 μm and 60 s of acquisition time. The estimated probe dimension in the plane xy is 77.4 μm .

at the entrance and exit ends is characterized by the Gaussian profile. At first approximation, ruling out the contributions due to the nonhomogeneous thickness of the 5 μm gold sheet and possible aplanarity of the sample, the dimension along the z -axis has been evaluated to be $\leq 98 \mu\text{m}$.

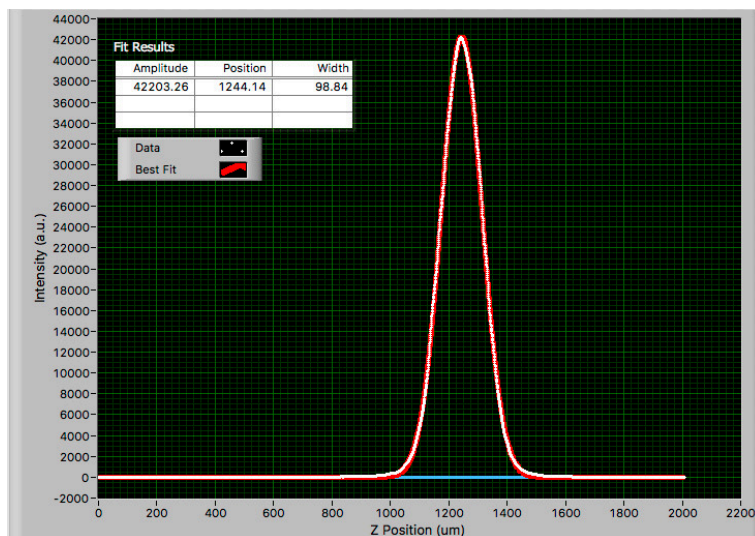


Figure 3. The linear μ XRF scan along the z -axis at 10 μm step. The estimated probe dimension in the z axis is $\sim 98 \mu\text{m}$.

2.3 Detection limit

As aforementioned the RXR station is characterized by two independent detection systems. The knowledge of the X-ray emission spectrum is a prerequisite in order to perform an accurate quantitative analysis, although it is difficult to measure directly the intensity of the excited spectrum.

The primary spectrum from our X-ray source was recorded at the exit of a polycapillary optics using scattered X-rays from both an organic glass and water (figure 4). We have evaluated the transmission of the optics comparing the fluorescence intensities from the certified NIST standard SRM 610 (Trace Elements in glass) [30]. The measured elemental fluorescence intensity from potassium to uranium is shown in figure 5.

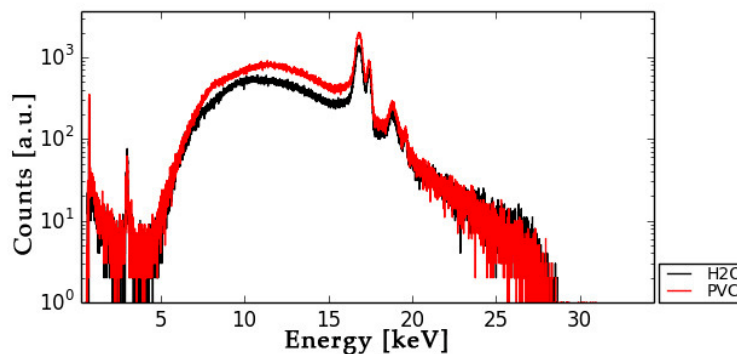


Figure 4. The excited spectra for a water (black) and an organic glass (red) recorded with polycapillary optics and 600 s counting time. The source parameters were fixed at 35 kV and 0.8 mA.

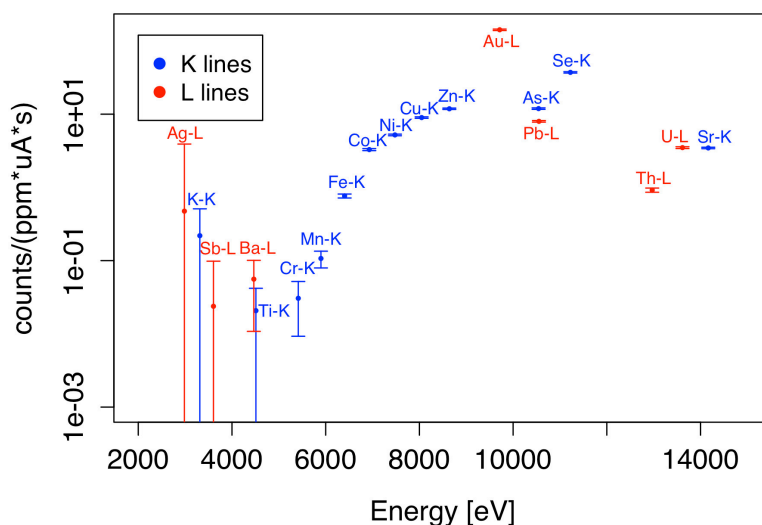


Figure 5. To evaluate the minimum concentration detection of the RXR station, the fluorescence elemental intensity of the NIST standard SRM 610 is shown. The trend points out the limited-efficiency of the detection system for the emission lines below 6 keV.

The trend showed points out the low efficiency of the “detection side” (semi-lens coupled with SDD) at low energy that affects the detection characteristic photons up to the iron element and photons corresponding to L-lines of heavy elements ($E < 6$ keV).

In varying of the NIST data a few measured elements (K-lines of K, Ti and Cr, and L-lines of Ag, Sb and Ba) have revealed a non-linear behavior with a low intensity and high fitting errors. Since the polycapillary lens of this confocal layout has been designed to cover the energy range from 6 to 30 keV this is the reason of the limited efficiency at low energy. As a consequence, a second confocal system with a different polycapillary semi-lens has been designed for the low energy. For quantitative analysis, we have evaluated the transmission of polycapillary optics by means of a Monte Carlo code [31, 32]. A further consideration deserves the Au element that we used to evaluate the minimum detectable concentration, i.e., $25 \pm 1.25 \mu\text{g/g}$.

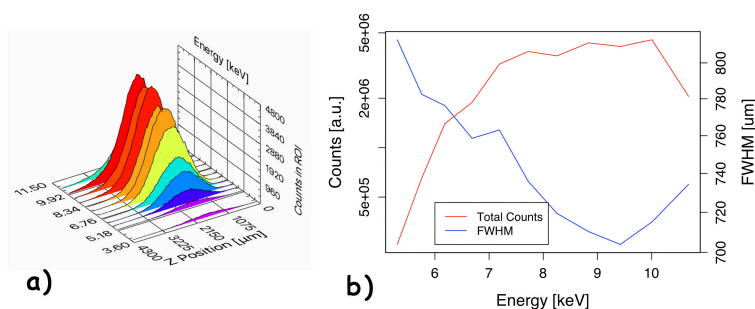


Figure 6. In the image a), from left to right the depth profile for Se, As, Ge, Ga, Zn, Cu, Ni, Co, Fe, Mn, Cr and Ca elements. In the b), for the same elements presented in a), it is showed the total counts and the FWHM of depth profile for each detected element.

To identify the parameters that characterize the confocal geometry in term of axial resolution, i.e., just beyond the surface without a full geometrical and physical degradation of the beam (figures 6 a and b), we select an intensity peak of 20% respect to the maximum. The penetration depth as a function of the radiation energy increases with the energy (figure 7).

The performances of the RXR experimental apparatus, i.e., the main geometrical and physical characteristics and the resolutions obtained by the analysis of both a thin wire and a foil are listed in table 1.

3 3D colour tomography

Conventional X-ray tomography techniques allow getting three-dimensional reconstructions, even of large objects, with sub-millimeter resolutions keeping high contrast for the objects composed by various inclusions of very different density. However, the information got are mostly morphological without any elemental data. At the same time, since conventional micro-fluorescence instruments do not utilize a confocal scheme, no bulk information, morphological and elemental information are provided.

Characterized by an ellipsoidal spot of $\sim 80 \div 90 \mu\text{m}$, RXR enables us in getting 3D bulk information. In order to show the confocal geometry capabilities as well as to discriminate volumes characterized by different densities and composition, we have investigated a sample, which includes a hard metallic piece surrounded by a soft solid media. Actually we have prepared a sample defined by a screw encapsulated in a drop of ethanol and methyl acetate glue. Unlike a classical tomography approach (CT scan), 3D- μXRF reconstruction has been performed collecting 2D scans on different

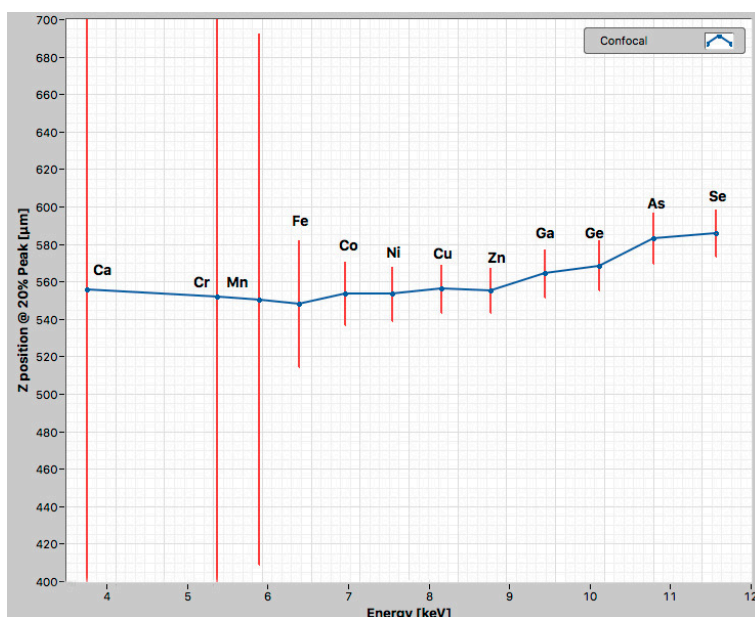


Figure 7. The experimental depth behaviour for a NIST standard considering the 20% of intensity after the maximum peak. As expected, the penetration increases for higher emission energy.

Analysis	μ XRF (2D/3D mapping) TXRF
X-ray source	Mo K — 50 W source spot $\sim 50 \mu\text{m}$
primary optics	polycapillary optics 90 μm spot size transmission: 22% @ Mo-K
secondary optics @ high en.	polycapillary semi-lens div. res.: 2.2 mrad transmission: 58 @ Cu-K
*) secondary optics @ low en.	polycapillary semi-lens div. res.: ~ 5 mrad transmission: $\sim 30\%$ @ Cu-K
detectors	SSD detectors active area: 25 mm^2 energy res.: $<135\text{eV}$ @ Mn-K
spot size in the plane xy-axis (wire 40 μm)	$\leq 77 \mu\text{m}$
spot size in z-axis (sheet 5 μm)	$\leq 98 \mu\text{m}$
min detectable concentration (Au-L)	$\sim 25 \pm 1.25 \mu\text{g/g}$

Table 1. Geometrical and physical RXR parameters. *) This option is presently under commissioning.

sections along the axial direction. In our measurements a total volume of $4.1 \times 4.1 \times 2.1 \text{ mm}^3$ was probed with a step of $100 \mu\text{m}$ ($\Delta x = \Delta y = \Delta z$) and acquisition period of 5 sec/step.

As an example, in figure 8 the images of two different layers, the first taken in the lower part of the sample volume and the second collected in the region corresponding to the screw end, have been compared clearly revealing three regions. The first two are due to the fluorescence of the metal screw presenting in the specimen and the radiation scattered by the soft matter. The last is a set of regions with no signal associated to the presence of air bubbles trapped during the hardening process of the glue. In the magnified image (figure 9) we have outlined the directions of the primary beam (excited radiation from the source-full lens to the sample) and the secondary beam (radiation from the sample — scattering, fluorescence, etc. . . — to the semilens-detector). The dotted lines identify the regions shadowed by the screw in this confocal geometry.

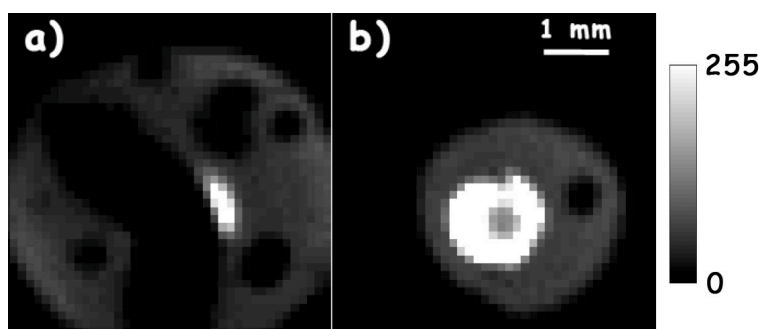


Figure 8. 2D scan of a metal screw encapsulated in the glue. Images refer to two different layers showing three different regions: a high fluorescence area due to the presence of the metal screw, a region associated to the primary radiation scattered by the glue and a signal-free region. a) The first layer refers to the lower volume of the 3D scan. b) The second layer has been obtained by scanning slightly below the top surface of the screw.

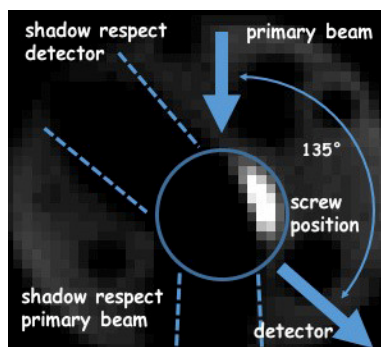


Figure 9. Magnified image of the layer in figure 8a where the directions of both primary beam and secondary radiation towards the detector have been highlighted. The angle between the two directions is 135° , obtained by the projection on the xy plane of the confocal geometry. The inner circle points out the location of the screw, while areas inside the dotted lines point out the shadow cones due to the metallic target.

Compared to tomography, the 3D μXRF technique allows the recognition of specific elemental contributions. As an example, in figure 10 a 3D rendering with the iron contribution outlined in red (b), the external surface of scattered beam (yellow) and the internal surface of the sample (grey) are

showed. This “elemental” visualization, with a spatial resolution of $\sim 100 \mu\text{m}$, clearly highlights the presence of bubbles (see white arrows “a” in figure 10) formed in the hardening process of the glue.

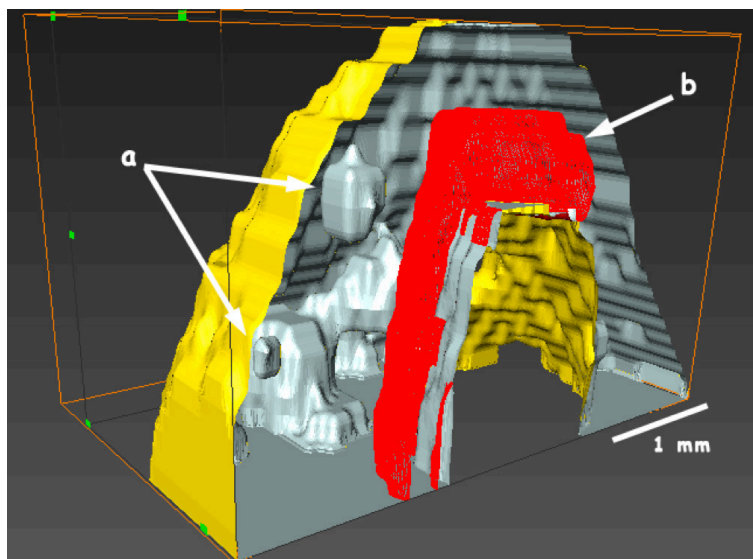


Figure 10. 3D reconstruction section of a screw encapsulated in the glue. The arrows a) and b) identify two air bubbles trapped during the hardening process of the glue.

4 Conclusions

This contribution describes characteristic and performances of the RXR apparatus for 2D/3D μXRF analysis. This unique spectroscopy unit based on a confocal geometry allows a depth profiling analysis with two different optical layouts optimized for high and low X-ray energy. Its design allows investigating large objects with lateral and axial spatial probe sizes of $80 \mu\text{m}$ each and a minimum detectable concentration of $25 \pm 1.25 \mu\text{g/g}$. To illustrate the capabilities, we have showed the image of a sample with mixture of strong and weak absorbing parts. Through the analysis of the primary scattered beam the porous structure of the matrix with a high spatial resolution have been reconstructed.

Presently we are working to commission our system with a second semi-lens coupled with a dedicated detector (with AP3.7 polymeric window). This option allows extending the fluorescence spectrum down to about 1 keV. Samples will be measured in vacuum down to 10^{-5} mbar. The vacuum chamber hosts a hexapod micro-positioner, which allows translations along six axes with a lateral resolution of $2.5 \mu\text{m}$ and an angular resolution of 1 mrad [33]. Dedicated polycapillary optics could be installed inside the chamber for fluorescence measurements at grazing angle (GIXRF/TXRF) and for X-ray imaging. This option will be described in a separate work. The availability of two different semi-lenses enables us to carry out simultaneous measurements both in air for the high Z elements ($Z > 15$) and in vacuum for low Z elements ($Z > 8$).

In addition to the existing experimental activities at the XLab Frascati, the RXR unit devoted to X fluorescence spectroscopy enhances the portfolio of experimental table top opportunities. The development of this quite original experimental instrument dedicated to micro-fluorescence, 2D

and 3D mapping and to the analysis of low concentrations samples by means of TXRF in the energy range from 1 to 30 keV may respond to three specific demands:

- a) preliminary tests of materials/samples for experiments using dedicated instruments available in large synchrotron radiation (SR) facilities;
- b) less demanding experiments in particular in terms of concentrations. Due to the large number of applications, these projects have low probability to receive beamtime at SR facilities, e.g., cultural heritage and geo-physical and geo-chemistry proposals;
- c) relatively compact instrument for “in situ” analysis of “samples”, which cannot be moved from their original locations or that do not fit the space available of the experimental stations of the existing SR facilities.

Acknowledgments

One of the authors (SBD) acknowledges the support by the Competitiveness Program of NRNU MEPhI. YuMC gratefully acknowledge the support of a fellowship of the Russian Federation President of the Ministry of Education and Science of the Russian Federation and the Competitiveness program of the Tomsk Polytechnic University.

References

- [1] R.V. Grieken and A. Markowicz, *Handbook of X-Ray Spectrometry*, 2nd ed., Marcel Dekker, New York (2002).
- [2] D. Hampai, S.B. Dabagov, G. Cappuccio, A. Longoni, T. Frizzi, G. Cibin et al., *Elemental mapping and microimaging by x-ray capillary optics*, *Opt. Lett.* **33** (2008) 2743.
- [3] O. Scharf, S. Ihle, I. Ordavo, V. Arkadiev, A. Bjeoumikhov, S. Bjeoumikhova et al., *Compact pnCCD-based x-ray camera with high spatial and energy resolution: A color x-ray camera*, *Anal. Chem.* **83** (2011) 2532.
- [4] F.P. Romano, C. Caliri, L. Cosentino, S. Gammino, L. Giuntini, D. Mascali et al., *Macro and micro full field x-ray fluorescence with an x-ray pinhole camera presenting high energy and high spatial resolution*, *Anal. Chem.* **86** (2014) 10892.
- [5] K. Tsuji, J. Injuk and R. Van Grieken, *X-Ray Spectrometry: Recent Technological Advances*, Wiley (2004).
- [6] D. Attwood, *Soft X-Rays and Extreme Ultraviolet Radiation: Principles and Applications*, Cambridge University Press (2007).
- [7] B. De Samber, G. Silversmit, K. de Schamphelaere, R. Evens, T. Schoonjans, B. Vekemans, *Element-to-tissue correlation in biological samples determined by three-dimensional X-ray imaging methods*, *J. An. At. Spect.* **25** (2010) 544.
- [8] K. Laclavetine, F.J. Ager, J. Arquillo, M.Á. Respaldiza and S. Scrivano, *Characterization of the new mobile confocal micro x-ray fluorescence (CXRF) system for in situ non-destructive cultural heritage analysis at the CNA: μ XRF-CONCHA*, *Microchem. J.* **125** (2016) 62.

- [9] K. Tsuji, K. Nakano and X. Ding, *Development of confocal micro x-ray fluorescence instrument using two x-ray beams*, *Spectrochim. Acta* **B 62** (2007) 549.
- [10] T. Nakazawa and K. Tsuji, *Development of a high-resolution confocal micro-XRF instrument equipped with a vacuum chamber*, *X-Ray Spectrom.* **42** (2013) 374.
- [11] S. Smolek, T. Nakazawa, A. Tabe, K. Nakano, K. Tsuji, C. Strelí et al., *Comparison of two confocal micro-XRF spectrometers with different design aspects*, *X-Ray Spectrom.* **43** (2013) 93.
- [12] G. Buzanich, P. Wobrauschek, C. Strelí, A. Markowicz, D. Wegrzynek, E. Chinea-Cano et al., *A portable micro-x-ray fluorescence spectrometer with polycapillary optics and vacuum chamber for archaeometric and other applications*, *Spectrochim. Acta* **B 62** (2007) 1252.
- [13] B. Kanngießer, W. Malzer, I. Mantouvalou, D. Sokaras and A. G. Karydas, *A deep view in cultural heritage—confocal micro x-ray spectroscopy for depth resolved elemental analysis*, *Appl. Phys. A* **106** (2011) 325.
- [14] L. Lühl, I. Mantouvalou, I. Schaumann, C. Vogt and B. Kanngießer, *Three-dimensional chemical mapping with a confocal XRF setup*, *Anal. Chem.* **85** (2013) 3682.
- [15] J.M. Feldkamp, C.G. Schroer, J. Patommel, B. Lengeler, T.F. Günzler, M. Schweitzer et al., *Compact x-ray microtomography system for element mapping and absorption imaging*, *Rev. Sci. Instrum.* **78** (2007) 073702.
- [16] G. Buzanich, P. Wobrauschek, C. Strelí, A. Markowicz, D. Wegrzynek, E. Chinea-Cano et al., *PART II (Portable ART analyzer)-development of a XRF spectrometer adapted for the study of artworks in the Kunsthistorisches Museum, Vienna*, *X-Ray Spectrom.* **39** (2010) 98.
- [17] S. Smolek, B. Pemmer, M. Fölser, C. Strelí and P. Wobrauschek, *Confocal micro-x-ray fluorescence spectrometer for light element analysis*, *Rev. Sci. Instrum.* **83** (2012) 083703.
- [18] M. Kumakhov, *Multiple reflection from surface x-ray optics*, *Phys. Rep.* **191** (1990) 289.
- [19] S.B. Dabagov, *Channeling of neutral particles in micro- and nanocapillaries*, *Phys. Usp.* **46** (2003) 1053.
- [20] <http://www.lnf.infn.it/xlab>.
- [21] D. Hampai, S.B. Dabagov and G. Cappuccio, *Advanced studies on the Polycapillary Optics use at XLab Frascati*, *Nucl. Instrum. Meth.* **B 355** (2015) 264.
- [22] D. Hampai, F. Bonfigli, S.B. Dabagov, R. Montereali, G. Della Ventura, F. Bellatreccia et al., *LiF detectors-polycapillary lens for advanced x-ray imaging*, *Nucl. Instrum. Meth.* **A 720** (2013) 113.
- [23] D. Hampai et al., *2D-3D μ XRF elemental mapping of archeological samples*, *Nucl. Instrum. Meth.* **B 402** (2017) 274.
- [24] L. Vincze, B. Vekemans, F.E. Brenker, G. Falkenberg, K. Rickers, A. Somogyi et al., *Three-dimensional trace element analysis by confocal x-ray microfluorescence imaging*, *Anal. Chem.* **76** (2004) 6786.
- [25] N. Zoeger, C. Strelí, P. Wobrauschek, C. Jokubonis, G. Pepponi, P. Roschger et al., *Determination of the elemental distribution in human joint bones by SR micro XRF*, *X-Ray Spectrom.* **37** (2008) 3.
- [26] <http://www.micro-epsilon.com/displacement-position-sensors/laser-sensor/>.
- [27] <http://www.xglab.it/compact-x-ray-sdd-spectrometer-xgl-spcm-8100.shtml>.
- [28] W. Malzer and B. Kanngießer, *A model for the confocal volume of 3d micro x-ray fluorescence spectrometer*, *Spectrochim. Acta* **B 60** (2005) 1334.

- [29] T. Schoonjans, G. Silversmit, B. Vekemans, S. Schmitz, M. Burghammer, C. Riekel et al., *Fundamental parameter based quantification algorithm for confocal nano-x-ray fluorescence analysis*, *Spectrochim. Acta B* **67** (2012) 32.
- [30] <https://www-s.nist.gov/srmors/certificates/610.pdf>.
- [31] R. Padilla, P.V. Espen, A. Abrahantes and K. Janssens, *Semiempirical approach for standardless calibration in μ -XRF spectrometry using capillary lenses*, *X-Ray Spectrom.* **34** (2004) 19.
- [32] K. Tsuji, T. Matsuno, Y. Takimoto, M. Yamanashi, N. Kometani, Y.C. Sasaki et al., *New developments of x-ray fluorescence imaging techniques in laboratory*, *Spectrochim. Acta B* **113** (2015) 43.
- [33] <https://www.physikinstrumente.com/en/>.